

# Fast parallel interferometric 3D tracking of numerous optically trapped particles and their hydrodynamic interaction

Dominic Ruh, Benjamin Tränkle, and Alexander Rohrbach\*

Laboratory for Bio- and Nano- Photonics, Department of Microsystems Engineering-IMTEK,  
University of Freiburg, Georges Köhler Allee 102, 79110 Freiburg, Germany

\*rohrbach@imtek.de

**Abstract:** Multi-dimensional, correlated particle tracking is a key technology to reveal dynamic processes in living and synthetic soft matter systems. In this paper we present a new method for tracking micron-sized beads in parallel and in all three dimensions – faster and more precise than existing techniques. Using an acousto-optic deflector and two quadrant-photo-diodes, we can track numerous optically trapped beads at up to tens of kHz with a precision of a few nanometers by back-focal plane interferometry. By time-multiplexing the laser focus, we can calibrate individually all traps and all tracking signals in a few seconds and in 3D. We show 3D histograms and calibration constants for nine beads in a quadratic arrangement, although trapping and tracking is easily possible for more beads also in arbitrary 2D arrangements. As an application, we investigate the hydrodynamic coupling and diffusion anomalies of spheres trapped in a  $3 \times 3$  arrangement.

©2011 Optical Society of America

**OCIS codes:** (120.0120) Instrumentation, measurement, and metrology; (290.0290) Scattering; (140.7010) Laser trapping; (260.3160) Interference

---

## References and links

1. M. W. Allersma, F. Gittes, M. J. deCastro, R. J. Stewart, and C. F. Schmidt, “Two-dimensional tracking of ncd motility by back focal plane interferometry,” *Biophys. J.* **74**(2), 1074–1085 (1998).
2. H. Kress, E. H. K. Stelzer, D. Holzer, F. Buss, G. Griffiths, and A. Rohrbach, “Filopodia act as phagocytic tentacles and pull with discrete steps and a load-dependent velocity,” *Proc. Natl. Acad. Sci. U.S.A.* **104**(28), 11633–11638 (2007).
3. J. C. Crocker and D. G. Grier, “Microscopic measurement of the pair interaction potential of charge-stabilized colloid,” *Phys. Rev. Lett.* **73**(2), 352–355 (1994).
4. A. van Blaaderen, J. P. Hoogenboom, D. L. J. Vossen, A. Yethiraj, A. van der Horst, K. Visscher, and M. Dogterom, “Colloidal epitaxy: playing with the boundary conditions of colloidal crystallization,” *Faraday Discuss.* **123**, 107–119, discussion 173–192, 419–421 (2003).
5. J. Dobnikar, M. Brunner, H.-H. von Grünberg, and C. Bechinger, “Three-body interactions in colloidal systems,” *Phys. Rev. E Stat. Nonlin. Soft Matter Phys.* **69**(3), 031402 (2004).
6. H. Kress, J. G. Park, C. O. Mejean, J. D. Forster, J. Park, S. S. Walse, Y. Zhang, D. Q. Wu, O. D. Weiner, T. M. Fahmy, and E. R. Dufresne, “Cell stimulation with optically manipulated microsources,” *Nat. Methods* **6**(12), 905–909 (2009).
7. A. Candelli, G. J. L. Wuite, and E. J. G. Peterman, “Combining optical trapping, fluorescence microscopy and micro-fluidics for single molecule studies of DNA-protein interactions,” *Phys. Chem. Chem. Phys.* **13**(16), 7263–7272 (2011).
8. J. C. Crocker, J. A. Matteo, A. D. Dinsmore, and A. G. Yodh, “Entropic attraction and repulsion in binary colloids probed with a line optical tweezer,” *Phys. Rev. Lett.* **82**(21), 4352–4355 (1999).
9. N. B. Becker, S. M. Altmann, T. Scholz, J. K. Hörber, E. H. Stelzer, and A. Rohrbach, “Three-dimensional bead position histograms reveal single-molecule nanomechanics,” *Phys. Rev. E Stat. Nonlin. Soft Matter Phys.* **71**(2), 021907 (2005).
10. M. L. Gardel, M. T. Valentine, J. C. Crocker, A. R. Bausch, and D. A. Weitz, “Microrheology of entangled F-actin solutions,” *Phys. Rev. Lett.* **91**(15), 158302 (2003).
11. J. Liphardt, S. Dumont, S. B. Smith, I. Tinoco, Jr., and C. Bustamante, “Equilibrium information from nonequilibrium measurements in an experimental test of Jarzynski’s equality,” *Science* **296**(5574), 1832–1835 (2002).

12. H. Kress, E. H. K. Stelzer, G. Griffiths, and A. Rohrbach, "Control of relative radiation pressure in optical traps: application to phagocytic membrane binding studies," *Phys. Rev. E Stat. Nonlin. Soft Matter Phys.* **71**(6), 061927 (2005).
13. I. M. Tolić-Nørrelykke, E. L. Munteanu, G. Thon, L. Oddershede, and K. Berg-Sørensen, "Anomalous diffusion in living yeast cells," *Phys. Rev. Lett.* **93**(7), 078102 (2004).
14. J. C. Meiners and S. R. Quake, "Direct measurement of hydrodynamic cross correlations between two particles in an external potential," *Phys. Rev. Lett.* **82**(10), 2211–2214 (1999).
15. R. Di Leonardo, S. Keen, F. Ianni, J. Leach, M. J. Padgett, and G. Ruocco, "Hydrodynamic interactions in two dimensions," *Phys. Rev. E Stat. Nonlin. Soft Matter Phys.* **78**(3), 031406 (2008).
16. J. Baumgartl and C. Bechinger, "On the limits of digital video microscopy," *Europhys. Lett.* **71**(3), 487–493 (2005).
17. M. Speidel, A. Jonás, and E. L. Florin, "Three-dimensional tracking of fluorescent nanoparticles with subnanometer precision by use of off-focus imaging," *Opt. Lett.* **28**(2), 69–71 (2003).
18. Z. Zhang and C.-H. Menq, "Three-dimensional particle tracking with subnanometer resolution using off-focus images," *Appl. Opt.* **47**(13), 2361–2370 (2008).
19. S.-H. Lee, Y. Roichman, G.-R. Yi, S.-H. Kim, S.-M. Yang, A. van Blaaderen, P. van Oostrum, and D. G. Grier, "Characterizing and tracking single colloidal particles with video holographic microscopy," *Opt. Express* **15**(26), 18275–18282 (2007).
20. F. C. Cheong, B. J. Krishnatreya, and D. G. Grier, "Strategies for three-dimensional particle tracking with holographic video microscopy," *Opt. Express* **18**(13), 13563–13573 (2010).
21. M. F. Juette and J. Bewersdorf, "Three-dimensional tracking of single fluorescent particles with submillisecond temporal resolution," *Nano Lett.* **10**(11), 4657–4663 (2010).
22. R. Bowman, G. Gibson, and M. Padgett, "Particle tracking stereomicroscopy in optical tweezers: control of trap shape," *Opt. Express* **18**(11), 11785–11790 (2010).
23. A. Pralle, M. Prummer, E. L. Florin, E. H. Stelzer, and J. K. Hörber, "Three-dimensional high-resolution particle tracking for optical tweezers by forward scattered light," *Microsc. Res. Tech.* **44**(5), 378–386 (1999).
24. A. Rohrbach, C. Tischer, D. Neumayer, E. L. Florin, and E. H. K. Stelzer, "Trapping and tracking a local probe with a Photonic Force Microscope," *Rev. Sci. Instrum.* **75**(6), 2197–2210 (2004).
25. R. Huang, I. Chavez, K. M. Taute, B. Lukic, S. Jeney, M. G. Raizen, and E.-L. Florin, "Direct observation of the full transition from ballistic to diffusive Brownian motion in a liquid," *Nat. Phys.* **7**(7), 576–580 (2011).
26. L. Friedrich and A. Rohrbach, "Improved interferometric tracking of trapped particles using two frequency-detuned beams," *Opt. Lett.* **35**(11), 1920–1922 (2010).
27. M. Speidel, L. Friedrich, and A. Rohrbach, "Interferometric 3D tracking of several particles in a scanning laser focus," *Opt. Express* **17**(2), 1003–1015 (2009).
28. K. Ubrig, R. Kurre, C. Schmitz, J. E. Curtis, T. Haraszti, A. E. M. Clemen, and J. P. Spatz, "Optical force sensor array in a microfluidic device based on holographic optical tweezers," *Lab Chip* **9**(5), 661–668 (2009).
29. A. Rohrbach, H. Kress, and E. H. K. Stelzer, "Three-dimensional tracking of small spheres in focused laser beams: influence of the detection angular aperture," *Opt. Lett.* **28**(6), 411–413 (2003).
30. K. C. Neuman and S. M. Block, "Optical trapping," *Rev. Sci. Instrum.* **75**(9), 2787–2809 (2004).
31. A. Rohrbach, "Stiffness of optical traps: quantitative agreement between experiment and electromagnetic theory," *Phys. Rev. Lett.* **95**(16), 168102 (2005).
32. A. Rohrbach and E. H. K. Stelzer, "Three-dimensional position detection of optically trapped dielectric particles," *J. Appl. Phys.* **91**(8), 5474–5488 (2002).
33. J. K. G. Dhont, *An Introduction to Dynamics of Colloids* (Elsevier, 1996).
34. E. R. Dufresne, T. M. Squires, M. P. Brenner, and D. G. Grier, "Hydrodynamic coupling of two brownian spheres to a planar surface," *Phys. Rev. Lett.* **85**(15), 3317–3320 (2000).
35. J.-C. Meiners and S. R. Quake, "Direct Measurement of Hydrodynamic Cross Correlations between Two Particles in an External Potential," *Phys. Rev. Lett.* **82**(10), 2211–2214 (1999).
36. S. Henderson, S. Mitchell, and P. Bartlett, "Direct measurements of colloidal friction coefficients," *Phys. Rev. E Stat. Nonlin. Soft Matter Phys.* **64**(6), 061403 (2001).
37. R. Di Leonardo, S. Keen, F. Ianni, J. Leach, M. J. Padgett, and G. Ruocco, "Hydrodynamic interactions in two dimensions," *Phys. Rev. E Stat. Nonlin. Soft Matter Phys.* **78**(3), 031406 (2008).
38. G. K. Batchelor, "Diffusion in a dilute polydisperse system of interacting spheres," *J. Fluid Mech.* **131**(-1), 155–175 (1983).

---

## 1. Introduction

Position tracking of particles has gained tremendous interest during the last years since a particle's trajectory  $\mathbf{r}(t)$  delivers an image of the interaction with its environment. Tracking diffusing particles in soft matter systems and deriving local interactions is of extreme importance in biology [1,2], chemistry [3,4] physics [5,6] and a variety of technical disciplines [6,7]. For slow processes or processes in thermal equilibrium, the histograms of the particle's tracked positions enable recovering the underlying landscape of free energy  $G(\mathbf{r})$  or forces  $\nabla G(\mathbf{r})$ , which also include enthalpic and entropic processes [8]. The faster and more precise a tracking method is, the more reliable and precise the histogram can be generated,

which often represents a good approximation of the particles probability density function  $p(\mathbf{r})$ . The precision of a tracking system defines the resolution  $\Delta\mathbf{r}$  of the position histogram or of  $p(\mathbf{r})$  [9], which can be down to a few nanometers and which is usually independent of the optical resolution  $\delta x \approx \lambda/2$  of a conventional microscope. From  $p(\mathbf{r})$  the landscape of free energy  $G(\mathbf{r}) = k_B T \cdot \ln(p(\mathbf{r})) + \text{const.}$  can be derived ( $k_B T \approx 4 \cdot 10^{-21}$  J is the thermal energy).

A fast and precise tracking system is even more indispensable for measuring dynamic interactions such as in micro-rheology [10] or for processes out of thermal equilibrium [11]. In this case analysis of correlations [12] or of power spectral densities allows the measurement of processes inside living cells [13], or more specifically, the hydrodynamic interaction of particles in a fluid [14,15].

Although a great variety of technical attempts have been made in the last years, it is still an ambitious, unachieved goal to track many particles in parallel in 3D at nanometer precision and at rates of several kilohertz. For the case of trapped particles, this would allow in addition to calibrate each optical trap independently and in 3D.

The most direct approach to reach this goal is to use a fast camera and to determine the center of mass of the particles image (video tracking) [16]. Although several methods have been proposed to determine also the exact axial position of the particle by focus blur analysis [17,18], by holographic techniques [6,19,20] or structured illumination [21,22], axial tracking is a profound drawback of camera based methods. In axial direction the precision is significantly worse than in the lateral directions and/or is not robust against changes of the local environment, since the fit-functions required to analyze the diffraction patterns on the camera often change with the environments refractive index and the plane of focus.

On the other side, techniques based on position sensitive devices, such as back-focal plane (BFP) interferometry are 1-3 orders of magnitude faster than video tracking [23–25]. In addition, BFP interferometry enables the very easy concept of calibrating the detector by the Langevin method, where 1-5 seconds of diffusions time are enough to determine the proportionality between signal and particle displacement in all three dimensions [24]. Although the axial tracking range of BFP interferometry is shorter than with some video tracking techniques, it has been extended to several particle diameters by various techniques [12,26] - sufficient for most optical trapping applications and still offering unmatched axial tracking precisions of 1-5 nm.

3D tracking of multiple particles in the kilo-Hertz range and individual trap calibration has been achieved recently by BFP interferometry of spheres in a time-multiplexed optical line trap [27], and for particles trapped with holographic optical tweezers (HOT) by digital holographic tracking [20], or in 2D by video tracking [28]. However, 3D tracking in the range of several kHz or faster of dozens of particles has not been achieved yet. This would allow determining position cross-correlations of hydrodynamic or nano-mechanically coupled particles, which would enable new insights into correlated soft matter systems and cell biology.

In this paper we present a method, where time multiplexed optical tweezers can trap  $N$  different particles in  $N$  traps and determine their 3D positions by using sequential BFP interferometric tracking (here  $N = 9$ ). This enables an independent calibration of both particle displacements and optical forces of  $N$  different particles in  $N$  different traps within seconds. Due to the high tracking rate of  $100/N \approx 11$  kHz, we show cross-correlation results of many particle hydrodynamic couplings.

## 2. Experimental configuration

Trapping and tracking of multiple particles is achieved by a self-made photonic-force-microscope (PFM) as described in principle in [24] and in [27]. Arbitrary focus and trap arrangements in a single plane have been achieved by time-multiplexing with help of a two-axis acousto-optic deflector (AOD) as schematically shown in Fig. 1(a). The optical path of the PFM comprises of a 2W 1064nm light source (Smart Laser Systems, Berlin), which passes first an optical isolator FI (OFR-IO-3-1064-VHP, Laser 2000), a beam expander and then the AOD subsequently (DTSXY-400, AA Opto-Electronic). The transmittances of the AOD are controlled to obtain long-term laser stability and specific laser intensity in every focus. A feedback-loop adjusts the transmittance of the X-AOD with respect to the low pass filtered (miniNE, TEM Messtechnik) intensity signal of an InGaAs photodiode (G8370-81, Hamamatsu Photonics), whereas a preamplifier (TEM Messtechnik) provides the required driving current to control the transmittance of the Y-AOD and therefore the power in every focus. A telecentric lens system (AC80, AC250) magnifies the AOD aperture on the BFP of the objective lens OL (UPLAPO60X/IR, Olympus) as outlined in Fig. 1(a). The OL creates the different time-shared foci in the object plane with discrete distances  $dx$  and  $dy$ . The interference pattern of the unscattered and the forward scattered laser light by the particle is projected via a detection lens DL (44069, Carl Zeiss) and two different  $4f$  lens systems (not shown, defining the spatial filter function  $H(k_x, k_y)$  in Eq. (1)) onto two quadrant-photo-diodes (QPDs). The two QPDs (G6849, Hamamatsu Photonics) differ in their effective numerical aperture  $NA$  to increase the signal quality for all three dimensions [26]. Silica beads with diameters of  $0.623\mu\text{m}$  and  $1.16\mu\text{m}$  were used in the experiments (SiO<sub>2</sub>-F-31000, SiO<sub>2</sub>-F-B1060, Microparticles GmbH) as shown in the image of Fig. 1(b).

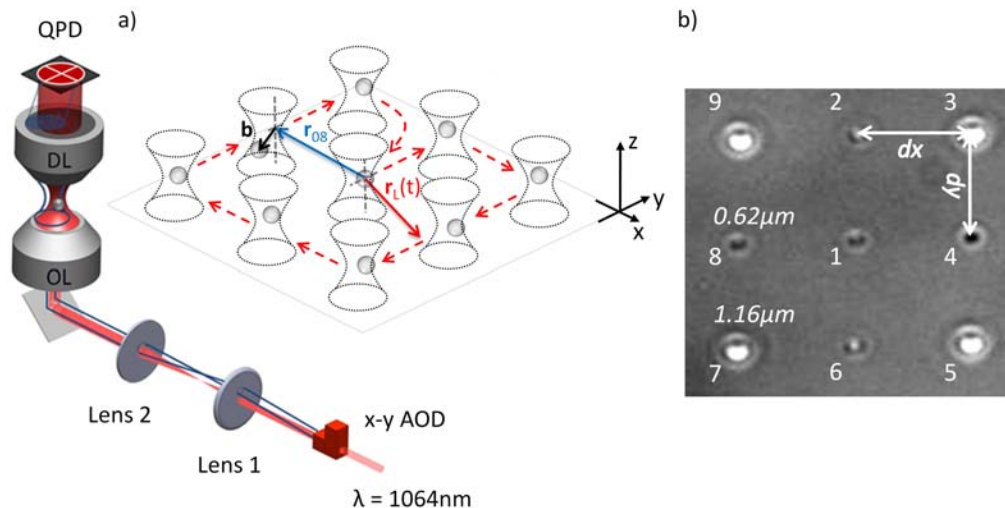


Fig. 1. Principle of setup and laser displacement scheme. (a) The aperture of a 2D-acousto-optic deflector (AOD) is imaged telecentrically on the BFP of the objective lens (OL), leading to a displacement of the trapping and tracking beam in the focal plane of the OL. For each beam center position  $r_l(t)$  and particle position  $b$ , the DL projects scattered and unscattered light for a short time onto the QPD. The sequence of beam displacements across all 9 particles begins with the central particle #1 ( $r_{08}$  indicates the center of the 8-th focus). (b) Brightfield image of four  $1.16\mu\text{m}$  and five  $0.62\mu\text{m}$  trapped glass beads separated by adjustable distances  $dx$  and  $dy$ . Bead numbers are indicated nearby each bead image.

### 3. Sequential interferometric tracking in the back focal plane

**Tracking Principle.** A single laser focus is time-multiplexed with a two-axis acousto-optic deflector (AOD) to create  $N$  optical traps with high stability in all three dimensions. As indicated in Fig. 1(a), the laser focus sequentially scans the mean positions of  $N$  particles, rests for a short time  $\tau_{on}$  at each position and thereby creates  $N$  effective optical potentials in arbitrary 2D arrangements. During the time  $\tau_{on}$  the position  $\mathbf{b}_n(t_0)$  of the  $n$ -th sphere ( $n \leq N$ ) at a specific time point  $t_0$  is determined. By varying the AOD transmission and thereby the laser intensity at each individual trap position, the potential depth and the trap stiffnesses can be adjusted very flexibly. For example, trap rearrangements during an experiment and online trap calibrations are possible.

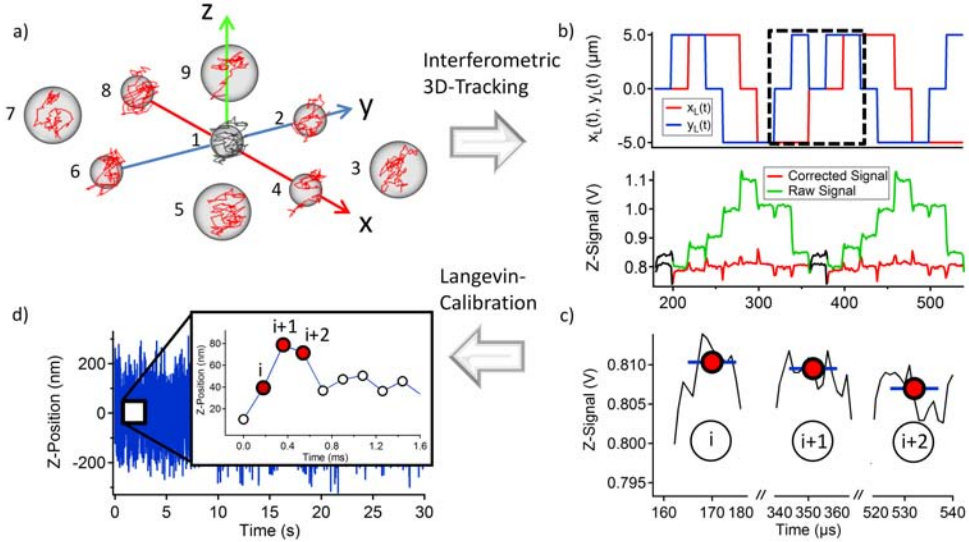


Fig. 2. Principles of sequential particle tracking. (a) Sketch of nine particles of different sizes arranged in the  $xy$ -plane. The exemplary diffusion paths (red and black) represent experimentally obtained data. (b) Upper graph: Focus displacements  $x_L(t)$  and  $y_L(t)$  as a function of time for the bead arrangement displayed in a). Lower Graph: Corresponding QPD signals for the particle  $z$ -positions. The piece of signal trajectory of the center particle #1 is drawn in black. (c) The sample points (red)  $i$ ,  $i + 1$ ,  $i + 2$  of the particle trajectory #1 are derived by averaging (blue) over ten centered signal points of the raw signal (black) to eliminate high frequency fluctuations ( $>70$  kHz) of the AOD. (d) Resulting axial position trajectory of particle #1, where the inset shows  $i = 9$  single positions. Three positions with red markers, which are derived from the periods  $i$ ,  $i + 1$ ,  $i + 2$  in (c), are highlighted.

The QPD detection system tracks intensity and position changes of the beads with frequencies of  $f_{\text{det}} = 1$  MHz (limited only by the pre-amplifiers), whereas the AOD varies the focus position and intensity, i.e. the trap arrangement at a maximum beam steering frequency of about  $f_{\text{AOD}} = 150$  kHz. At the frequency  $f_{\text{AOD}} / N$  the 3D position of  $N$  spheres by BFP interferometry can be tracked precisely, as we will explain in the following.

**Signal acquisition and correction.** In BFP-interferometry a QPD measures an intensity signal  $\hat{S}_n(\mathbf{b})$  on its  $m$ -th quadrant with area  $A_m$  placed in the BFP or a conjugate plane ( $k_x, k_y$ ) of a detection lens. The interference intensity  $\hat{S}^m(\mathbf{b}, \mathbf{r}_L)$  from the incident field  $\tilde{\mathbf{E}}_{0,n}$  at position  $\mathbf{r}_L$  and the field  $\tilde{\mathbf{E}}_{s,n}(\mathbf{b}_n)$  scattered at the  $n$ -th particle at position  $\mathbf{b}_n(t)$  can be written as [24,27]

$$\hat{S}^m(\mathbf{b}_i, \mathbf{r}_L) = \iint_{A_m} \left| \tilde{\mathbf{E}}_{0,n}(k_x, k_y, \mathbf{r}_L) + \tilde{\mathbf{E}}_{s,n}(k_x, k_y, \mathbf{b}_n, \mathbf{r}_L) \right|^2 \cdot H(k_x, k_y) dk_x dk_y \quad (1)$$

The function  $H(k_x, k_y)$  represents a spatial filter, which increases the tracking quality [29]. From a linear combination of the 4 raw signals  $\hat{S}^1(\mathbf{b}) \dots \hat{S}^4(\mathbf{b})$ , the signal triplet  $\mathbf{S}(\mathbf{b}) = (S_x(\mathbf{b}), S_y(\mathbf{b}), S_z(\mathbf{b}))$  encoding the spheres center position  $\mathbf{b}$  can be obtained. The positions of the laser focus are denoted by  $\mathbf{r}_L(t) = (x_L(t), y_L(t), z_L = 0)$ , whereas the center position of the  $n$ -th particle  $\mathbf{b}_n(t) = (b_{n,x}(t), b_{n,y}(t), b_{n,z}(t))$  can be assumed to be linear with the measured  $n$ -th signal intensity  $\mathbf{S}_n(t) = (S_{n,x}(t), S_{n,y}(t), S_{n,z}(t))$  [24] as long as particle displacements from the  $n$ -th trap center are smaller than their diameter, such that

$$\begin{aligned} \mathbf{S}_n(t) &= \mathbf{S}_n^{\text{raw}}(t) / c_n - \mathbf{S}_{0n}(t) \\ &\approx \left( (g_{n,x} \cdot b_{n,x}(t)), (g_{n,y} \cdot b_{n,y}(t)), (g_{n,z} \cdot b_{n,z}(t) + S_{0n}(t)) \right) - \mathbf{S}_{0n}(t) \\ &\approx \bar{\mathbf{g}}_n \circ \mathbf{b}_n(t) \end{aligned} \quad (2)$$

The ability of adjusting the laser intensity in every trap individually is shown by a recursive algorithm that reduces the laser intensity by a factor  $1/c_n$  in every trap towards the lowest measured  $z$ -signal (where  $c_n = 1$ ). The factor  $1/c_n$  accounts for the deflection dependent intensity transmission of an AOD. By subtracting the signal mean  $\mathbf{S}_{0n}(t)$  from the corrected (normalized) signal  $\mathbf{S}_n^{\text{cor}}(t) = \mathbf{S}_n^{\text{raw}}(t) / c_n$ , we end up with the signal  $\mathbf{S}_n(t)$  (see Fig. 2(b)).  $\bar{\mathbf{g}}_n$  is approximately a diagonal matrix, where the elements  $g_{n,x}, g_{n,y}, g_{n,z}$  represent the detector sensitivities of the  $n$ -th particle in the directions  $x, y$  and  $z$ .

Figure 2(a) shows exemplarily an array of  $N = 9$  spheres of different sizes arranged in the  $xy$ -plane with distances  $d_{nx}$  and  $d_{ny}$  to each other. The nine trajectories  $\mathbf{b}_n(t)$  in red and black denote the displacements relative to the  $n$ -th trap center, which is at  $\mathbf{b}_{0n}$ , slightly behind the center of the  $n$ -th laser focus  $\mathbf{r}_n$ . Therefore the stepwise displacement of the laser focus relative to the  $n$ -th trap center  $\mathbf{r}_{n,\text{rel}} = \mathbf{r}_{0n} - \mathbf{r}_L(t)$  can be expressed e.g. in  $x$ -direction and for constant jumps  $d_{nx} = d_x$ , as

$$x_{\text{rel},n} = x_{0n} - x_L(t) = -d_x + \sum_{n=0}^{N'} d_x \cdot \Theta(t - n \cdot \Delta t) \quad (3)$$

A Heaviside step function  $\Theta(t)$  describes the jumps of length  $d_x$  from one focus position to the other after the time  $\Delta t$ . For particles in a row,  $N'$  in Eq. (3) is limited to the number of  $x$ -steps in one row (see dotted region in Fig. 2(b) where  $N' = 1$ ,  $d_x = 5\mu\text{m}$  and  $\Delta t = 20\mu\text{s}$ ). Both  $x_{\text{rel}}(t)$  and  $y_{\text{rel}}(t)$  are plotted in Fig. 2(b) together with the measured  $z$ -signals for all nine particles and over 2 scans with time period  $\tau_{\text{scan}}$ . The scan duration  $\tau_{\text{scan}}$  is given by  $N$  times the time  $\Delta t$  between two jumps

$$\tau_{\text{scan}} = N \cdot \Delta t = \tau_{\text{on}} + \tau_{\text{off}} = 1 / f_{\text{AOD}} + (N - 1) \cdot \Delta t. \quad (4)$$

The time, the laser is located at the  $n$ -th position can be approximated by  $\tau_{\text{on}} \approx 1 / f_{\text{AOD}} = \Delta t$ , since the time to jump from position  $x_i$  to  $x_{i+1}$  is negligibly small ( $i$  counts the number of scans of all  $N$  particles). We further call the time the laser is off the  $n$ -th particle  $\tau_{\text{off}} = (N - 1) \cdot \tau_{\text{on}}$ . The ratio between  $\tau_{\text{on}}$  and  $\tau_{\text{off}}$  also defines the effective, i.e. time-averaged strength of each optical trap. Time-averaged, effective optical forces will be further explained in the next section.

**Extracting the trajectory of a single particle.** The position signals as e.g.  $S_z(t) \approx g_z \cdot b_z(t)$  shown in Fig. 2(b) are governed by the Brownian motion of the optically trapped particles. This motion can be described by a stochastic equation of motion, the Langevin equation, where the  $x$ -component reads:

$$\gamma \cdot \dot{b}_{n,x}(t) + F_{\text{opt},n,x}(x_L, b_{n,x}(t)) = F_{\text{th}}(t) \quad (5)$$

In this over-damped situation terms of inertia are neglected.  $\dot{b}_{n,x}(t)$  is the velocity of the  $n$ -th particle diffusing in x-direction. The drag coefficient for spherical particles derived from Stokes law is  $\gamma = 6\pi\eta(T)R$ , with temperature  $T$  dependent viscosity  $\eta$  and the radius of the particle  $R$ .  $F_{th}$  is the thermal force, which is discussed later in this paper and  $F_{opt,n,x}$  is the optical force in x-direction of the  $n$ -th optical trap. This trapping force vanishes for a position  $b_{0n}$ , which defines the trap center, such that  $F_{opt,n}(b_{0n}) = 0$ , where  $b_{0n} = 0$  in x-direction.

The position and signal fluctuations become visible in Fig. 2(c) and Fig. 2(d). Each particle has its own trajectory with time sequence  $t_n = i \cdot \tau_{scan} + n \cdot \tau_{on}$  and is sampled in the time interval  $\tau_{scan} = N/f_{AOD}$ . The period  $\tau_{on}$  is in the range of some  $\mu\text{s}$  and represents 2 times the period, over which a mean position is measured (see Fig. 2(c)). These average values, indicated as red markers  $i, i+1, i+2$  for subsequent points in time, constitute the position trajectory  $\bar{S}_{n,j}(t_n)$  of the  $n$ -th particle in direction  $j = (x,y,z)$

$$\begin{aligned} \bar{S}_{n,j}(i \cdot \tau_{scan} + n \cdot \tau_{on}) \\ = \bar{S}_{n,j}(t_n) = \frac{1}{\tau_{on}/2} \cdot \int_{t_n + \tau_{on}/4}^{t_n + 3\tau_{on}/4} S_{n,j}(t' + t_n) dt' = g_{n,j} \cdot b_{n,j}(t) \end{aligned} \quad (6)$$

In our case, a constant offset of  $8\mu\text{s}$  between the desired x-y position of the laser ( $x_L(t), y_L(t)$ ) and the QPD signals arises because of the time the acoustic wave has to propagate through the Bragg-cell of the AOD. This temporal offset is already corrected in (Fig. 2(b)). Since the beam deflection frequency we chose for all experiments was  $f_{AOD} = 50 \text{ kHz}$ , the laser remained for  $\tau_{on} \approx 20\mu\text{s}$  at every bead and returned after  $\tau_{scan} = 180\mu\text{s}$ . At a detector sample rate of  $f_{det} = 1 \text{ MHz}$ ,  $\tau_{on}$  corresponds to 20 sample points. From these, we extracted the mean value of the 10 centered sample points over a time interval of  $\tau_{on}/2$  as illustrated by Fig. 2(c) and indicated in Eq. (6). The other ten points in every period are discarded because the peaks that arise from the beam steering via the AOD falsify the position of the bead. Taking the average of 10 points of a particle diffusing with e.g. a diffusion constant  $D \approx 0.5\mu\text{m}^2/\text{s}$ , this effectively suppresses diffusion lengths of about  $\sqrt{\langle b_j^2 \rangle} = (2 \cdot k_B T / \gamma \cdot \tau_{on}/2)^{1/2} \approx (1\mu\text{m}^2/\text{s} \cdot 10\mu\text{s})^{1/2} \approx 3\text{nm}$ , which are negligibly small. This averaging effect occurs with any standard detector with an integration time of  $10\mu\text{s}$  and a sampling rate of  $(180\mu\text{s})^{-1} = 5.5 \text{ kHz}$ . Finally it is important to emphasize, that the tracking precision is the same as for standard BFP interferometry, which is between 1 and 5 nm in all 3 directions [24].

#### 4. Parallelized force and position calibration

In this section we briefly recapitulate how to calibrate a sphere in a static point trap. From this we can derive the change in forces and calibration constants for  $N$  particles in  $N$  time-multiplexed traps.

Calibration of optical tweezers means to determine the proportionality factor  $\kappa_j$  (trap stiffness) in the linear range of the optical force  $F_j \approx \kappa_j \cdot b_j$  as a function of particle displacement  $b_j$  in all three directions  $j = x,y,z$ . Depending on the calibration method [30], very often also the detection system (particle tracking system) needs to be calibrated, such that we seek the detector sensitivity  $g_j$  in the linear signal range  $S_j \approx g_j \cdot b_j$  as introduced in Eq. (2).

**Force calibration of a static point trap.** When using the popular Langevin method for calibrating both the trap and the detector, the equipartition theorem is necessary, which relates the thermal energy to the degrees of freedom of a particle at thermal equilibrium. For a particle trapped in a harmonic potential with stiffness  $\kappa_j$  one finds for the mean square displacement  $\langle b_j^2 \rangle = \sigma_j^2$  of the particle:

$$\kappa_j \cdot \langle b_j^2 \rangle = k_B T \quad (7)$$

The trap stiffness  $\kappa_j$  is the characteristic quantity for a particle diffusing in a harmonic optical trapping potential  $V(b_j)$ , with a potential depth of several times the thermal energy  $k_B T$ . Provided  $\gamma$  is known,  $\kappa_j$  is obtained via the auto-correlation time  $\tau_j = \gamma / \kappa_j$ , which can be determined easily from a fit to the exponentially decaying auto-correlation function  $AC(\tau)$  of the signal trajectory,

$$AC(S_j(t)) = \langle S_j(t) \cdot S_j(t+\tau) \rangle = (\sigma_j^{sig})^2 \cdot \exp(-\tau \cdot \kappa_j / \gamma), \quad \kappa_j = \gamma / \tau_j \quad (8)$$

As a rule of thumb, the sampling interval  $\tau_{scan}$  should be least  $m \approx 5$  times shorter than the auto-correlation time  $\tau_j \approx m \cdot \tau_{scan}$  of the trap, to enable a reliable exponential fit to Eq. (8).

**Position distribution.** The variance  $\langle b_j^2 \rangle = \sigma_j^2$  of the position distribution in Eq. (7) can be determined from the width of the resulting particle's Gaussian probability density distribution (PDF)  $p(b_j) = p_0 \cdot \exp(-V(b_j) / k_B T)$ , if the system is in thermal equilibrium:

$$p(b_j) \approx p_0 \cdot \exp(-\frac{1}{2} \kappa_j b_j^2 / k_B T) = p_0 \cdot \exp(-\frac{1}{2} b_j^2 / \sigma_j^2) \quad (9)$$

The PDF or approximated, the position histogram, has a Gaussian shape in all three spatial directions. In the next section, it will be discussed, how the optical forces and the width of the PDF effectively change, when the optical potential is  $V(b_j) = 0$  during the time  $\tau_{off}$  when the focus is off the particle. Under the condition that the restoring forces are linear time and then independent of  $\tau_{off}$ , the shape of the PDF (histogram) remains Gaussian for a time-multiplexed trap as pointed out by Fig. 3, which shows 9 x 3 point clouds from position fluctuations of 9 spheres, which were trapped and tracked in parallel.

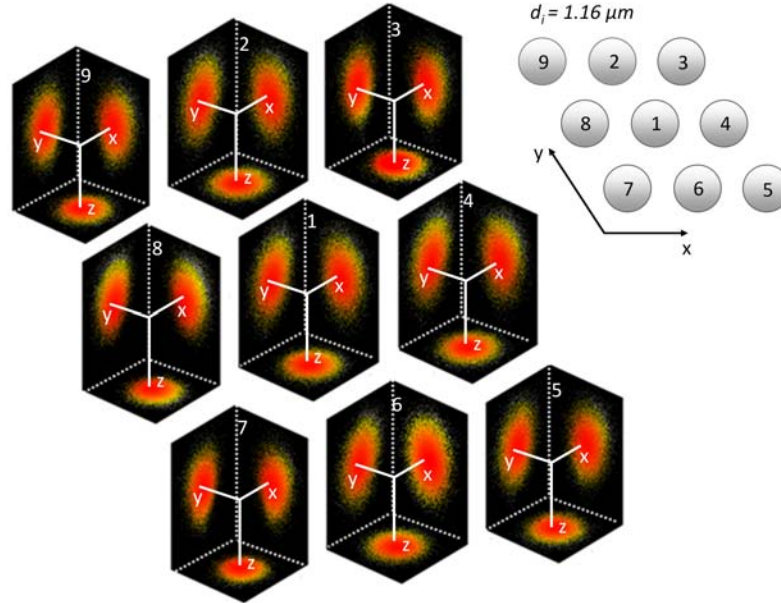


Fig. 3. Projections of particle trajectories measured in parallel in a point cloud representation. Projections are shown in x-, y- and z-direction for all 9 particles trajectories. The symmetric shape and nearly identical extensions of the clouds reflect the well-defined adjustment of individual trapping strengths in the trap array. All glass spheres have a diameter of 1.16 $\mu$ m.

**Detector calibration of a static and a multiplexed trap.** Since not only  $S_j$  and  $b_j$  are proportional to each other, but also the standard deviations of the signal PDF  $\sigma_j^{sig}$  and the position PDF  $\sigma_j$ , i.e.  $\sigma_j = g_j \cdot \sigma_j^{sig}$ , we end up with the detector sensitivity  $g_j$  in direction  $j = x, y, z$ :

$$g_j = \frac{\sigma_j^{sig}}{\sigma_j} = \sigma_j^{sig} \cdot \sqrt{\frac{\kappa_j}{k_B T}} \quad (10)$$

Equation (10) is standard when finding the detector sensitivity in ( $V/\mu\text{m}$ ) via the Langevin calibration method and provides the exact position  $b_j$ , as long as the laser power and the trap stiffness  $\kappa_j$  do not change over the on-time  $\tau_{on}$ . In the following, it will be shown that Eq. (10) is also valid for a time-multiplexed trapping and tracking system.

The question to be discussed is how the optical force, the potential and the PDF change, when the system is out of equilibrium, specifically when the laser beam is not at the particle during the time period  $\tau_{off}$  and only applies forces during the period  $\tau_{on}$ .

**Theoretical estimate of the effective trap stiffness.** The optical force on a small particle can be estimated more easily if scattering forces can be neglected and gradient forces dominate. If we assume an intensity distribution in the focus  $|E_i(x)|^2 = I(x) = I_0 \cdot \exp(-x^2/\Delta_x^2)$  in the lateral direction with a full width half maximum (FWHM)  $\Delta_x = 0.5 \cdot \lambda/NA$  in the focus defined by the NA of the trapping lens, the gradient force  $F_{grad}(b_x)$  of a point trap can be approximated for spheres with diameter  $D \leq \lambda$  as

$$\begin{aligned} F_{grad}(b_x) &= \frac{\alpha n}{2cV} \int_{V(\text{bead})} \nabla I(\mathbf{r} - b_x \cdot \mathbf{e}_x) dV = \frac{\alpha n}{2cV} \cdot \int \nabla I(\mathbf{r} - b_x \cdot \mathbf{e}_x) \cdot s(\mathbf{r}) dV \\ &\approx \frac{\alpha n}{2c} \frac{\partial}{\partial b_x} \left( I_0 \cdot \exp\left(-\left(b_x / \Delta_x'\right)^2\right) \right) \Big|_{b_x \ll \Delta_x} \approx -\kappa_x \cdot b_x \end{aligned} \quad (11)$$

with polarizability  $\alpha$  ( $[\alpha] = \text{m}^3$ ), with speed of light  $c/n$  in a medium with refractive index  $n = 1.33$  and the sphere's shape function with  $s(\mathbf{r}) = 1$ , if the bead radius is  $R > |\mathbf{r}|$ ,  $s(\mathbf{r}) = 0$  otherwise. For small particle displacements  $b_x$  in the trap center, the linear approximation  $F_{grad} \approx -\kappa_x \cdot b_x$  is justified. The integral in Eq. (11) corresponds to a 1D convolution along  $x$  between the intensity gradient of the focus  $\nabla I(\mathbf{r})$  and the shape function of the bead  $s(\mathbf{r})$ ,  $\nabla I(\mathbf{r}) * s(\mathbf{r})$ , and thereby to a profile broadening to  $\Delta_x' \approx \Delta_x + 2R$  by roughly the diameter of the bead. From Eq. (11) we find the lateral stiffness of a point trap to be  $\kappa_x \approx I_0 \cdot \alpha \cdot n / (c \cdot \Delta_x'^2)$ .

Since the center of the laser focus is at the relative position  $\mathbf{r}_{rel}(t) = (x_{rel}(t), y_{rel}(t), 0)$  the force  $F_{grad}(b_x - x_{rel})$  needs to be calculated at the lateral position  $b_x - x_{rel}$ . For distances  $|b_x - x_{rel}| > \Delta_x'$  such as the jump distance  $d_x$ , the particle does not see the force profile and  $F_{grad}(b_x - x_{rel}) = 0$ . Inserting the time-dependent laser position of Eq. (3) into Eq. (11) we find

$$F_{grad}(b_x, x_{rel}(t)) \approx \begin{cases} V_0 \cdot \frac{\partial}{\partial b_x} \exp\left(-\frac{(b_x - x_{rel}(t))^2}{\Delta_x'^2}\right) & \text{if } |b_x - x_{rel}(t)| \leq \Delta_x' \\ 0 & \text{otherwise} \end{cases} \quad (12)$$

with energy  $V_0 = I_0 \cdot \alpha \cdot n / c$  and  $[V_0] = \text{Nm}$ . To determine the effective, time-averaged optical force acting on a particle in a time-multiplexed trap, we have to integrate over one scan period  $\tau_{scan} = \tau_{on} + \tau_{off} = \Delta t + (N-1) \cdot \Delta t$ ,

$$\begin{aligned}
F_{eff}(b_x) &= \frac{1}{N\Delta t} \left( -\frac{2V_0}{\Delta_x'^2} \right) \cdot \underbrace{\int_0^{\Delta t} b_x \cdot \exp\left(-\frac{(b_x-0)^2}{\Delta_x'^2}\right) dt}_{=const \cdot \Delta t} \\
&+ \frac{1}{N\Delta t} \left( -\frac{2V_0}{\Delta_x'^2} \right) \cdot \underbrace{\int_0^{(N-1)\Delta t} \underbrace{(b_x - x_{rel}(t))}_{\approx d_x > \Delta_x'} \cdot \exp\left(-\frac{(b_x(t) - x_{rel}(t))^2}{\Delta_x'^2}\right) dt}_{=0}
\end{aligned} \tag{13}$$

The second term vanishes, because it describes the case, the trap is located at one of the other  $N-1$  particles (Eq. (12)). The first integrand does not depend on  $t$  and is constant. The first term considers the case the laser is at the particle over the period  $\Delta t$ . Simplification of Eq. (13) results in an expression, where the effective force is a factor  $1/N = \tau_{on}/\tau_{scan}$  (see Eq. (4)) weaker than the optical gradient force with constant laser intensity:

$$\begin{aligned}
F_{eff}(b_x) &= \frac{1}{N} \left( -\frac{2V_0}{\Delta_x'^2} \right) \cdot b_x \cdot \exp\left(-\frac{b_x^2}{\Delta_x'^2}\right) \\
&= \frac{1}{N} \cdot F_{grad}(b_x) = \frac{\tau_{on}}{\tau_{on} + \tau_{off}} \cdot F_{grad}(b_x) \stackrel{b_x \ll \Delta_x'}{\approx} -\kappa_{x,eff} \cdot b_x
\end{aligned} \tag{14}$$

This result is intuitive, but it should be mentioned that Eq. (12) holds also for small distances  $d_x$ , i.e. where adjacent traps overlap and the force distributions become more complicated. The force slope is approximated linearly around its center. The effective trap stiffness for the time-multiplexed trap (with constant jumps  $\Delta t$ ) is obtained as

$$\kappa_{eff} = \frac{\gamma}{\tau_{eff}} = \frac{1}{N} \cdot \kappa = \frac{\tau_{on}}{\tau_{on} + \tau_{off}} \cdot \frac{I_0 \alpha n}{c \cdot \Delta_x'^2} \tag{15}$$

The time  $\tau_{on}$  the laser remains at one specific trap position can be precisely selected. According to Eq. (15) the effective trap stiffnesses can be controlled by the resting time  $\tau_{on}$  and the laser intensity  $I_0$ . For  $\tau_{off} > \tau_{on}$  the stiffness  $\kappa_{eff}$  can be kept constant, if the ratio  $I_0 / \tau_{off}$  is kept constant.

**Invariance of the detector sensitivity.** Inserting Eq. (15) into Eq. (9) we find a PDF of the trapped particle broadened by a factor  $N$ ,

$$p_{eff}(b_j) \approx p_0 \cdot \exp\left(-\frac{1}{2} b_j^2 / \sigma_{eff,j}^2\right) \quad \text{and} \quad \sigma_{eff,j} = \sqrt{N} \cdot \sigma_j \tag{16}$$

Inserting Eq. (15) into Eq. (10), which describes the detector calibration, we find that the time averaged detector sensitivity  $g_j = \sigma_{eff,j}^{sig} / \sigma_{eff,j} = (\sqrt{N} \cdot \sigma_j^{sig}) / (\sqrt{N} \cdot \sigma_j)$  remains the same since both histograms widths increase by a factor  $\sqrt{N}$ . The invariance of the detector sensitivity has been described already above.

**Laser intensity and scan frequency.** In frequency domain, the diffusion of an optically trapped particle can be described by its power-spectral density  $PSD(\omega) = |\tilde{x}(\omega)|^2 = |FT[x(t)]|^2 = FT[AC\{x(t)\}]$ ,  $FT[\ ] =$  Fourier-transform,  $AC\{\ \} =$  Auto-correlation [24]. Since the particle's PSD has a Lorentzian characteristic, confined diffusion can be technically described by a low-pass filter with corner frequency  $f_c = 1/\tau_0$  defined by the strength of the optical trap. Particles that are scanned and tracked with frequencies  $f_{scan} = 1/\tau_{scan} > f_c$  can be calibrated correctly inside their traps. i.e. are not affected by the beam multiplexing. Therefore the minimum scanning frequency  $f_{scan} = 1/(\tau_{on} + \tau_{off})$  can be estimated relative to the AOD-frequency, the

number of trapped particles, a factor  $q$  and the corner-frequency  $f_c = \kappa / \gamma$  of the optical traps with stiffness  $\kappa$ :

$$f_{scan} = \frac{1}{\tau_{on} + \tau_{off}} = \frac{f_{AOD}}{N} \geq q \cdot f_c \quad \text{or} \quad \tau_{scan} \leq \tau_0 / q \quad (17)$$

From a combination of Brownian dynamics simulations and optical force simulations [31], we found the factor to be minimal  $q = f_{scan} / f_c \geq 5$ . Therefore the scan rate was chosen to be 5 times larger than the trap's corner frequency in all experiments, except of the experiment described in Fig. 5. As shown, the corner frequency  $f_c$  or trap stiffness  $\kappa$  is proportional to the laser intensity and to the ratio of  $\tau_{on} / \tau_{off}$ . On the one hand the traps should not be too stiff, to ensure  $5f_c \leq f_{scan}$  on the other hand, the trap should not be too soft, to avoid diffusion of the particle out of the linear tracking regime [29].

## 5. Experimental results

We performed trapping and tracking experiments in an arrangement as described by Fig. 1. More precisely, we put four  $1.16\mu\text{m}$  sized and five  $0.62\mu\text{m}$  sized glass particles into an equally spaced nine trap arrangement with trap stiffnesses recursively calibrated such that the mean intensity of the z-signal was constant for all traps for better comparability. We recorded the position signals 25 times for 30 seconds and processed the raw-data (see Fig. 2(c)) to obtain the detector sensitivities  $g_j$  and the effective trap stiffnesses  $\kappa_{j,eff}$  ( $j = x, y, z$ ). The calculated mean value and the standard deviation for the calibration parameters are shown in Fig. 4. On the one hand, the different levels of  $\kappa_j$  and  $g_j$  for the two bead diameters are clearly visible in all directions. On the other hand, the small relative deviations for one nominal bead size show the well-aligned trap arrangement.

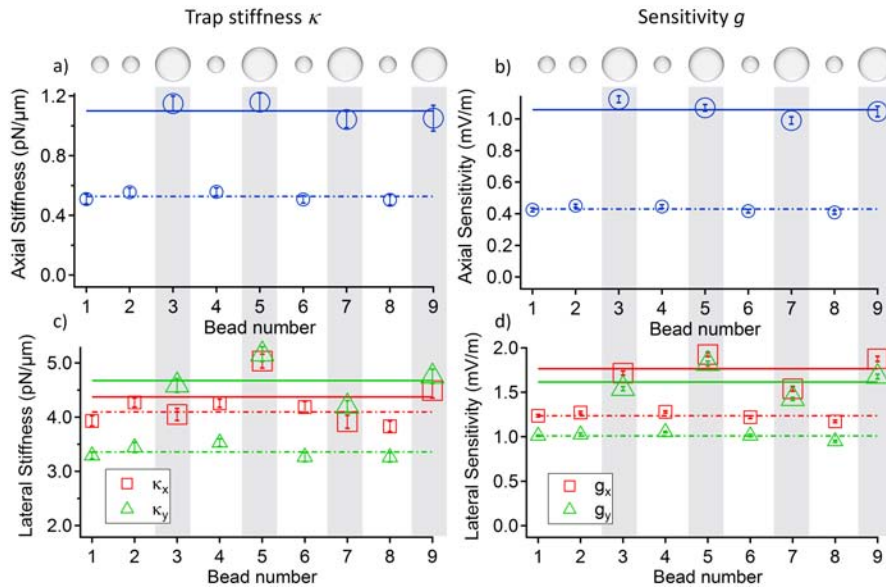


Fig. 4. Measured trap stiffnesses  $\kappa_j$  (a,c) and detector sensitivities  $g_j$  (b,d) ( $j = x, y, z$ ) from four  $1.16\mu\text{m}$  (big markers) and five  $0.62\mu\text{m}$  (small markers) trapped glass beads. The axial components are in the top row, the lateral in the bottom row. The markers are colored in red for the x-, in green for the y- and in blue for the z-direction. a,c) The trap stiffnesses are the same of each bead size in all three directions. Differences between x- and y- direction result from the polarization of the incident field. b,d) The detector sensitivities clearly reveal the two different bead radii in all three directions.

Small deviations are likely due to variations in AOD transmission (phase and amplitude) and of the bead size, where a constant radius  $R$  and drag  $\gamma = 6\pi\eta R = \kappa_{j,eff} \cdot \tau_{j,eff}$  was assumed. The small error bars indicate, that the measured detector sensitivities and trap stiffnesses are well reproducible over time and beam deflection area.

As predicted and measured in references [31,32] the trap stiffnesses in the y-direction are weaker  $\kappa_y < \kappa_x$  than in x-direction, since y is the direction of the polarization of the incident field. This polarization effect becomes smaller, when the diameter of the sphere reaches the diameter of the focus. However, differences in  $\kappa_j$  and  $g_j$  can be even much bigger, since each trap is calibrated individually and would deliver the same result for force measurements.

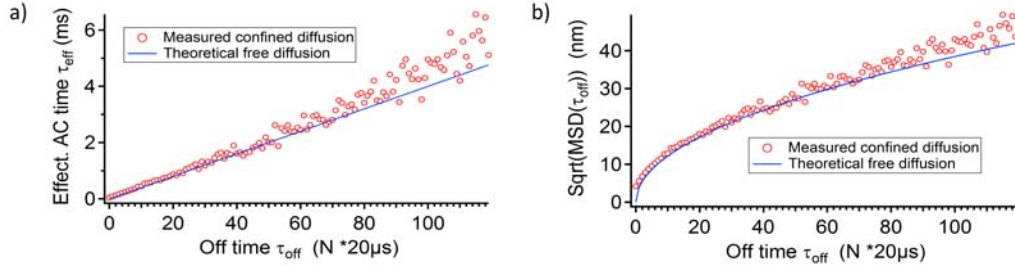


Fig. 5. (a) Increase in the effective auto-correlation (AC) time (left) and the rms-displacement of the particle (right). The AC-time increases linearly with the off-time  $\tau_{off} = N \cdot \tau_{on}$  (number of traps  $N = 0..120$ ). (b) The experimental data can be well approximated by the particle's expected free diffusion.

By a further experiment we show, that the theory of effective, time-averaged trap stiffnesses is valid for numerous trapped particles. Therefore a trap arrangement with 120 virtual traps was established, although only one particle was trapped. The time  $\tau_{on} = 20\mu s$  the laser remains at position of the trapped particle is kept constant, whereas the time  $\tau_{off}$  is increased linearly after every measurement with time increment  $\Delta t = \tau_{on}$ . The auto-correlation (AC) times predicted by Eq. (15) and obtained by the correlation analysis reveal in Fig. 5 left the expected proportionality between the effective AC time  $\tau_{eff}$  and the off-time  $\tau_{off}$ . For  $\tau_{off} = 0$  we find  $\tau_{eff} = \tau_x = \gamma / \kappa_x$  and for a number of  $N$  traps  $\tau_{eff}$  increases linearly:

$$\tau_{eff,x} = \left(1 + \tau_{off} / \tau_{on}\right) \cdot \tau_x = N \cdot \tau_x \approx 2 \cdot \tau_{off} \quad (18)$$

During  $\tau_{off}$  the freely diffusing particle has a mean square displacement  $MSD_{free}(\tau_{off}) = \sigma_{free}^2 = 2 \cdot k_B T / \gamma \cdot \tau_{off}$ . Assuming that the particle diffuses freely over  $N$  parts of the scan time and sees the trapping potential for only 1 part, free diffusion will mainly determine the width of the effective, time-averaged PDF, i.e.  $\sigma_{free}(\tau_{off}) \approx \sigma_{eff}(\tau_{off})$  or  $2\tau_{off} \cdot k_B T / \gamma \approx \tau_{eff} \cdot k_B T / \gamma$ . This behavior is clearly visible in Fig. 5, where the theoretical free diffusion  $MSD_{free}(\tau_{off}) = 2 \cdot k_B T / \gamma \cdot \tau_{off}$  is plotted with  $\tau_{eff} = 2 \cdot \tau_{off}$ . For the width  $\sigma_{eff} = (k_B T / \kappa_{eff})^{1/2}$  of the PDF, which remains of Gaussian shape, we find:

$$\sigma_{eff,x} = \sqrt{k_B T \cdot \tau_{eff,x} / \gamma} = \sqrt{1 + \tau_{off} / \tau_{on}} \cdot \sigma_x = \sqrt{N} \cdot \sigma_x \quad (19)$$

Here  $\sigma_x = (k_B T / \kappa_x)^{1/2} \approx 5\text{nm}$  is obtained from a strong static point trap with  $\kappa_x = 260\text{pN}/\mu\text{m}$  and  $\tau_x = 36\mu s$ . The measurement time was 10s each for every off-time  $\tau_{off}$ .

In the example presented in Fig. 3 with  $N = 9$  beads with each  $\tau_x = 0.25\text{ms}$  AC-time this corresponds to  $\tau_{off} = (9-1) \cdot \tau_{on} = 160\mu s$ ,  $\sigma_{free} = 11\text{nm}$  and an increase in PDF width by a factor  $(1 + 9/1)^{1/2} \approx 3.16$ .

## 6. Hydrodynamic coupling of particles in a two-dimensional array

As mentioned in the introduction, multi-particle tracking allows measuring force fields and physical coupling between confined areas in a complex soft-matter environment. In this section we show, how nine trapped particles change their temporal diffusion and fluctuation behavior due to hydrodynamic coupling over distances of several particle radii.

The diffusion behavior of  $N$  coupled particles can be described by  $N$  Langevin equations  $\tilde{\gamma}_{mn} \cdot \dot{\mathbf{r}}_n(t) + \mathbf{F}_{opt,n}(\mathbf{r}_n) = \mathbf{F}_{th,n}(t) \mathbf{F}$  as introduced by Eq. (5), which are coupled by the elements  $\tilde{\gamma}_{mn}$  of the viscous drag tensor  $\tilde{\gamma}$ . For the sake of convenience, we write the position of the  $n$ -th sphere as  $\mathbf{r}_n(t)$ , instead of  $\mathbf{b}_n(t)$ , and its velocity as  $\mathbf{v}_n(t) = \dot{\mathbf{r}}_n(t)$ . By further assuming linear effective optical forces  $F_{opt,n}(x_n) \approx \kappa_{nm} x_n$  for all trapped spheres, the system of Langevin equations reads:

$$\begin{pmatrix} \tilde{\gamma}_{11}(r) & \tilde{\gamma}_{12}(r) & \cdots & \tilde{\gamma}_{1n}(r) \\ \tilde{\gamma}_{21}(r) & \tilde{\gamma}_{22}(r) & \cdots & \tilde{\gamma}_{2n}(r) \\ \vdots & \vdots & \ddots & \vdots \\ \tilde{\gamma}_{m1}(r) & \tilde{\gamma}_{m2}(r) & \cdots & \tilde{\gamma}_{mn}(r) \end{pmatrix} \cdot \begin{pmatrix} \dot{\mathbf{r}}_1(t) \\ \dot{\mathbf{r}}_2(t) \\ \vdots \\ \dot{\mathbf{r}}_n(t) \end{pmatrix} + \begin{pmatrix} \kappa_{11} & 0 & \cdots & 0 \\ 0 & \kappa_{22} & \cdots & 0 \\ \vdots & \vdots & \ddots & \vdots \\ 0 & 0 & \cdots & \kappa_{nn} \end{pmatrix} \cdot \begin{pmatrix} \mathbf{r}_1(t) \\ \mathbf{r}_2(t) \\ \vdots \\ \mathbf{r}_n(t) \end{pmatrix} = \begin{pmatrix} F_{th,1}(t) \\ F_{th,2}(t) \\ \vdots \\ F_{th,n}(t) \end{pmatrix} \quad (20)$$

The viscous drag matrix  $\tilde{\gamma}$  with elements  $\tilde{\gamma}_{mn}$  is inverse to the hydrodynamic mobility matrix  $\tilde{\mu}$  with elements  $\tilde{\mu}_{mn}$ . For a single spherical particle it simply reads  $\mu_0 = \mu_{nn} = 1/\gamma_{nn} = (6\pi\eta R)^{-1}$ .

In principle and according to Eq. (20) the viscous drag of each bead is influenced by all other  $(n-1)$  beads, such that the velocity dependent friction force of the  $m$ -th bead is  $\sum_n \tilde{\gamma}_{mn} \cdot \dot{\mathbf{r}}_n(t)$ . Since such a system is far too complex to describe, we reduce the complexity by considering first the hydrodynamic interaction between two adjacent spheres. For two isolated spheres at positions  $\mathbf{r}_n$  and  $\mathbf{r}_m$  in a distance  $r = |\mathbf{r}| = |\mathbf{r}_n - \mathbf{r}_m|$  to each other, the distance dependent mobility  $\tilde{\mu}_{mn}(r)$  is a tensor itself and can be split up in components for motions parallel and perpendicular to the center-to-center axis [33]:

$$\tilde{\mu}_{mn}(r) = \mu_{mn}^{\parallel}(r) \cdot \frac{\mathbf{r} \otimes \mathbf{r}}{r^2} + \mu_{mn}^{\perp}(r) \cdot \left(1 - \frac{\mathbf{r} \otimes \mathbf{r}}{r^2}\right) \quad (21)$$

Here  $\otimes$  denotes the outer product. For the simultaneous motion of both spheres at distances  $r > R$  one finds for the first order approximation after a transform into center-of-mass coordinates  $\mu_{rel}^{\parallel}(r) \approx \frac{1}{2}\mu_0 \cdot (1 - \frac{3}{2} \cdot R/r)$  and  $\mu_{rel}^{\perp}(r) \approx \frac{1}{2}\mu_0 \cdot (1 - \frac{3}{4} \cdot R/r)$  for relative motions between the beads. For the collective motion of both spheres one finds  $\mu_{col}^{\parallel}(r) \approx \frac{1}{2}\mu_0 \cdot (1 + \frac{3}{2} \cdot R/r)$  and  $\mu_{col}^{\perp}(r) \approx \frac{1}{2}\mu_0 \cdot (1 + \frac{3}{4} \cdot R/r)$ . Usually, relative diffusion between two spheres, expressed by the diffusion constant  $D_{rel} = \mu_{rel} \cdot k_B T$ , is slowed down with decreasing distance  $r$ , whereas collective diffusion is accelerated with decreasing  $r$  via  $D_{col} = \mu_{col} \cdot k_B T$  [34]. Typically, this two bead interaction is investigated by cross-correlations  $CC_i(\tau) = \langle x_{i,n}(t) \cdot x_{i,m}(t + \tau) \rangle$  of the positions of two spheres as a function of time delay  $\tau$  [35] [36]. This reads in directions  $i = x, y, z$ :

$$CC_i^{\parallel}(\tau) = \frac{k_B T}{2\kappa_i} \cdot \left( e^{-\tau\mu_0\kappa_i(1+\frac{3}{2}R/r)} - e^{-\tau\mu_0\kappa_i(1-\frac{3}{2}R/r)} \right) \quad (22)$$

$$CC_i^{\perp}(\tau) = \frac{k_B T}{2\kappa_i} \cdot \left( e^{-\tau\mu_0\kappa_i(1+\frac{3}{4}R/r)} - e^{-\tau\mu_0\kappa_i(1-\frac{3}{4}R/r)} \right) \quad (23)$$

In these expression we have assumed to have two identical spheres in two identical traps with stiffnesses  $\kappa_i = \kappa_{i,mm}$ . The cross-correlations are expressed by the difference of the auto-correlation functions of the collective movement with mobility  $\mu_{rel}$  and of the relative

movements with mobility  $\mu_{col}$ . Evaluating Eqs. (22) and (23) results in a negative cross-correlation curve, where  $e^{-\tau\mu_{col}K_i} \leq e^{-\tau\mu_{rel}K_i}$ , meaning that correlated fluctuations relax faster than anti-correlated fluctuations because of a larger mobility  $\mu_{col} > \mu_{rel}$  of the collective motion.

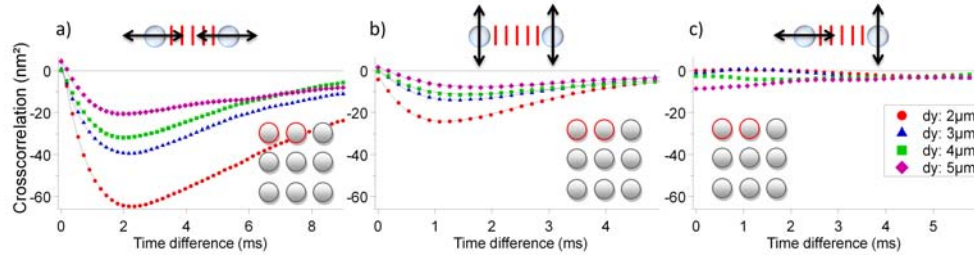


Fig. 6. Cross-correlation functions  $CC(\tau)$  for two  $1.16\mu\text{m}$  glass spheres (marked with red circles) in various distances  $r = dy$  to each other. (a) The strongest coupling is for longitudinal motions  $CC_{yy}(\tau)$ , weaker coupling for transversal motions  $CC_{xx}(\tau)$  (b) and negligible small coupling for motions in perpendicular directions  $CC_{xy}(\tau)$  (c). Coupling is strongest for short distances  $dy = 2\mu\text{m}$  with a time delay of  $\tau_{min} \approx 2\text{ms}$ . The particle arrangement is quadratic as pointed out in the insets.

Figure 6(a) shows the position cross-correlation of two adjacent spheres in longitudinal direction (Eq. (22)) for 4 different distances  $r = dy$  in the  $3 \times 3$  arrangement of Fig. 1. Figure 6(b) shows the position cross-correlation in transversal direction (Eq. (23)) and Fig. 6(c) shows the cross-correlation in perpendicular directions. To obtain this data, the trajectories  $x_{i,n}(t)$  of the  $n \leq 9$  particles in directions  $i = x, y, z$  have been tracked in parallel as described above. Figure 6(a) reveals, that the correlation strength is the stronger the shorter the distance between the spheres. For two isolated spheres, this effect was already shown in references [35], [36] and [37]. Meiners and Quake [35] also pointed out that the delay time, i.e. the minimum position  $\tau_{min}$  increases with decreasing distance (see dashed line in Fig. 6(a)), which is not intuitive and which is not further discussed here. In Fig. 6(b) it can be seen that in our case the coupling in transverse directions is about a factor 3 weaker than in longitudinal directions, whereas coupling in perpendicular directions is negligible (Fig. 6(c)). The maximum coupling strength is reached after half the time for the transversal motions as for the longitudinal motions.

Besides the coupling due to the three types of directional motions presented in Fig. 6, we investigate the case of a mediator bead between two trapped spheres. By plotting the position cross-correlation between two  $1.16\mu\text{m}$  glass spheres in a distance of  $dy = 4\mu\text{m}$  without an intermediate bead, we find a pronounced dip at a time delay of  $\tau_{min} = \tau_4 = 2\text{ms}$  as shown in Fig. 7. Placing a third bead in between, such that the distances are  $2\mu\text{m} + 2\mu\text{m}$ , we find a reduction of the interaction strength of the two outer beads by a factor of 3, but a remarkably decrease in the time delay by a factor of  $\tau_4 / \tau_{22} = 2$ . In other words: although a mediator bead damps the position fluctuations and the hydrodynamic coupling between two spheres, the maximum coupling between the outer spheres occurs much earlier.

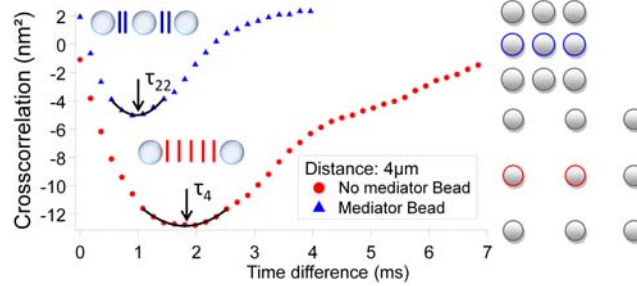


Fig. 7. (Color online) Cross-correlation functions  $CC(\tau)$  for two beads in a distance  $dy = 4\mu\text{m}$  to each other with and without mediator bead in between. The longitudinal coupling strength is increased without the mediator bead, but the delay time is reduced with mediator bead. The auto-correlation time of a single trapped bead was  $\tau_y = 7\text{ ms}$ , and  $\tau_y = 5\text{ ms}$ , respectively.

A well-known result in colloidal physics is that the diffusion of spheres change in dependence of the volume concentration of surrounding beads [38], where the long-time diffusion coefficient as a function of the volume fraction  $\varphi = a^2/r^2$  between bead radius  $a$  and bead distance  $r$  is estimated. As shown in Dhont [33], the normalized coefficient  $D' = D(r) / D(r \rightarrow \infty)$  of free diffusion decays as  $D'_{short} = 1 - 1.7\varphi$  for short times and  $D'_{long} = 1 - 2.1\varphi$  for long times. Figure 8 left illustrates that the normalized diffusion coefficient drops linearly according to  $D'_{trap} = 1 - 0.9\varphi$ , and is therefore less sensitive to neighbored beads on short time scales  $\tau_j \ll \gamma/\kappa_j$  as predicted. For time scales  $\tau_j \geq \gamma/\kappa_j$  the auto-correlation decay nearly exponentially. The decay is weaker than predicted by theory, since in our experimental arrangement only interactions in 2 dimensions and for next neighbors are incorporated. This decay is the weaker, the shorter the distances and the stronger the hydrodynamic coupling to the other beads. At a distance of  $r = 2\mu\text{m} = 1.7 \cdot a$ , we find  $D(r) = k_B T / \gamma(r) = 0.75 \cdot D(r \rightarrow \infty)$ , i.e. diffusion drops down by 25% due to the coupling to the beads.

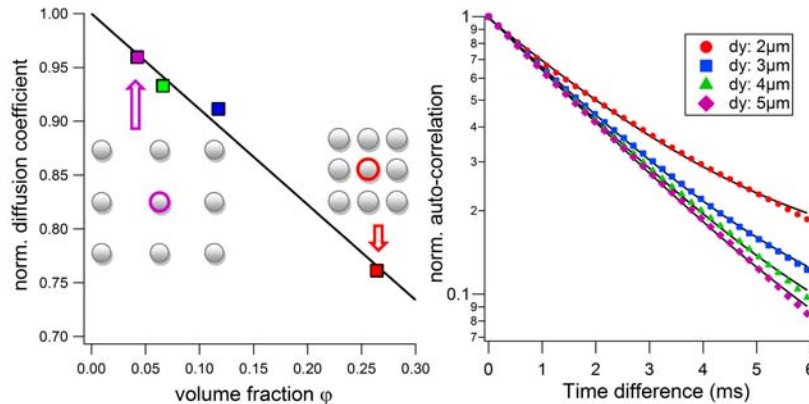


Fig. 8. Self-diffusion of the center bead as a function of distance to the beads. (a) Decay of the normalized diffusion coefficient as a function of volume ratio corresponding to decreasing distances  $dy$ . (b) Normalized auto-correlation function  $AC(\tau)$  of the center bead for 4 bead to bead distances  $r = dy$ .

## 7. Summary and conclusions

In this paper we have presented a novel 3D multi-particle tracking system with 20 $\mu$ s time resolution. The tracking principle and precision of 1-5nm is the same as for the established single beam systems using back-focal-plane (BFP) interferometry. Due to time-multiplexing with a two-axis acousto-optic deflector (AOD) the resting times at each particle are short ( $\sim$ 20 $\mu$ s), but have no influence on the tracking linearity and orthogonality of the x-, y- and z-position signals. The calibration of the traps and the position signals, i.e. determining the constants  $\kappa_{j,n}$  and  $g_{j,n}$  ( $j = x,y,z$ ) for each particle and laser focus with number  $n$ , is possible independently of local laser power, particle size and refractive index. Applying the established Langevin method for all  $N \times 3$  constituted traces ( $N = 9$  in our case), the  $N \times 3$  calibration constants  $\kappa_{i,n}$  and  $g_{i,n}$  can be obtained within seconds. This was shown for mixture of 0.62 $\mu$ m and 1.16 $\mu$ m glass beads with high reproducibility. The aforementioned features make our tracking system superior to any existing tracking system for the frequent case, that particles are trapped in a single z-plane. An extension of this work for trapping numerous particles in different z-planes using spatial light modulators in addition is in preparation.

We have shown theoretically and by experiments that effective, time-averaged trapping potentials arise, when the laser is on one particle during  $\tau_{on}$  and off the particle during  $\tau_{off}$ . The effective trap stiffness can be controlled generally by the ratio between the periods  $\tau_{on}$  and  $\tau_{off}$ , and, in addition for each trap individually by the laser power transmitted through the AOD.

We used the fast tracking system to record 27 position traces of nine trapped 1.16 $\mu$ m glass spheres, which represent a well-sized probe for many biological applications. From these traces we determined cross-correlations  $CC(\tau)$  between selected pairs of particles. These allowed us identifying various hydrodynamic coupling strengths and times between two spheres from the minima of the resulting  $CC(\tau)$ -curves. On the one hand we found similar results as those published by others for two isolated spheres, on the other hand we found unexpected hydrodynamic coupling between two spheres if a mediating sphere was in between. In addition we found that self-diffusion of the centered bead decreases linearly with decreasing distance to the eight surrounding beads. Without doubt, more experiments, more advanced theoretical approaches and different analysis are required to better understand many particle hydrodynamic coupling in regular and irregular particle arrangements. This is beyond the scope of this article.

The system principles presented here should be easily adaptable to standard trapping and tracking systems, which use BFP-interferometry and beam steering devices. The system features we presented will make it possible to not only measure 3D force fields, but also to steer defined forces at each point individually. We think that this ability will open doors to a variety of new exciting experiments in biophysics and related disciplines.

## Acknowledgment

This work was supported by the Deutsche Forschungsgemeinschaft (DFG), grant numbers RO 3615/1 and RO 3615/2. The authors thank Matthias Koch for a thorough of reading the manuscript.